Observation of a Large Population of Optical Scatterers in the Advanced LIGO mirrors

Lamar Glover[1], Michael Goff[1], Jignesh Patel[1], Innocenzo Pinto[2], Maria Principe[2], Travis Sadecki[3], R. L. Savage[3], Ethan Villarama[1],Eddy Arriaga[1], Erik Barragan[1], Riccardo DeSalvo[1,2], Eric Do[1], Cameron Fajardo[1],

[1]California State University, Department of Physics and Astronomy, 5151 State University Drive, Los Angeles CA 90032, USA[2]University of Sannio at Benevento, 82100 Benevento, Italy and INFN (Sezione di Napoli), Italy

[3]LIGO – Hanford Observatory, 127124 N Route 10, Richland, WA 99352, USA

e-mail address: lglover3@calstatela.edu

Similar in appearance to images of star clusters, photographs of the LIGO Gravitational Wave detector mirrors illuminated by the standing beam were analyzed with DAOPHOT, an astronomical software tool designed to identify stars within images and extract information about the structure of light point sources. DAOPHOT found hundreds of thousands of weaker, point-like scatterers, uniformly distributed across the mirror surface, ignoring the smear of actual dirt on the mirror. The amplitude distribution of the observed scatterers implies that they extend through the depth of the coating while their sheer number implies a fundamental, thermodynamic origin. Theoretical material science considerations indicate that these scatterers are a likely source of the mirror dissipation and thermal noise, perhaps pointing the way towards a mitigation strategy, improved sensitivity of Gravitational Wave observatories and increased Gravitational Wave detection radius into the Universe.

Keywords: optics, scattering, thermal noise, dissipation, quality factor, crystallites, gravitational waves

PACS: 95.55.Br, 95.55.Ym, 81.70.-q

I. INTRODUCTION

The mirror test masses of the LIGO Gravitational Wave detector[i,ii] have been specifically designed and constructed with multilayered interference coatings[iii] deposited via ion-beam deposition to minimize optical absorption, mirror thermal noise[iv,v] and light scattering[vi]. As such, an ideal mirror would appear black when viewed off axis from a collimated source of illumination. However, photographs of an Advanced LIGO End Test Mass illuminated by the 100 kW interferometer stored beam taken at a 9.8° angle from the stored beam axis (Figure 1) show a large number of light scattering points, which were initially interpreted as dirt. This investigation identified, in addition to dirt, hundreds of thousands of diffraction-limited, weak light scatterers, many per mm^2. The unexpectedly large number, and uniform dispersal of these scatterers is not compatible with dirt. Their brightness distribution suggests that they may be uniformly distributed in depth within the coating layers.

Since the overall absorption, measured by the mirror heating, is less than ¼ ppm, the relatively larger scattering must be a result of minuscule refraction index fluctuations that do not absorb energy. These density fluctuations are due to either denser proto-crystal formations or small, localized density deficits (atomic scale void clusters).

The uniform distribution, and the large number, imply that the scatterer generation happens during the deposition process itself and is likely of a thermodynamic or statistical nature. While these defects were observed in ion beam deposited glasses, it is important to note that molten glasses, such as the fused silica mirror substrate of the mirrors, are free of this kind of scatterers.

Ion beam deposited glass layers have been shown to have low quality factors, in the thousands, or tens of thousands, as compared with the many millions, or even billions, quality factors measured in high quality molten glasses [vii]. The mechanical losses associated with the lower quality factor of the coatings cause excess thermal noise in the mirror that, in turn, limits the sensitivity of gravitational waves detection[viii]. While recent results started giving indications[ix], thus far there has been no clear identification of the source of the excess dissipation in coating layers. It will be shown that the observed scatterers are a likely locus of the larger than expected coatings mechanical losses. While the exact nature of the light scatterers cannot be identified at this time, their observation is an important diagnostic tool to develop deposition procedures that mitigate optical scattering as well as thermal noise.

II. METHODS AND PROCEDURE

Using DAOPHOT[x], a software tool developed by the National Optical Astronomy Observatory[xi] to count stars in astronomical images, a large number of tiny scatterers, or irregularities in light reflection, have been detected within the mirror coating layers. The search tool is optimized to detect point-like objects, ignoring "nebula-like" dirt particles. The camera lens cannot resolve the points extracted by DAOPHOT. These points are compatible with, and are identified by their congruence with, Airy disk profiles generated by the camera lens aperture. Best fit procedure inside DAOPHOT was used to extract the position (in the X,Y plane) and amplitude information of each candidate in 40 images of varying exposure times that were acquired at the LIGO Hanford observatory.

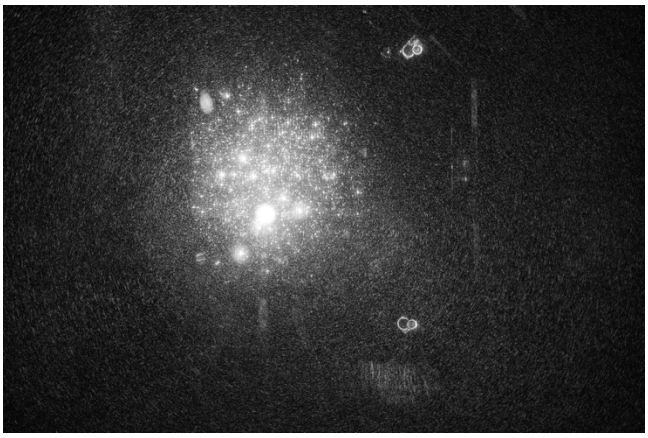

Figure 1. *November 2015 Photograph of an End Test Mass at LIGO Hanford with an exposure time of 1.3 seconds. Crowding in the image is solely due to the finite size and nature of the Airy disks. The actual scatterers are expected to be of sub-micron size and widely separated within the actual coating layers of the End Test Mass. (Note: The rings and faint straight lines that appear in the background on the right side of the image are components of the mirror support structure).*

There is a varying degree in scatterer image quality within the images, which can be attributed to either pixel saturation or scatterer crowding. The scatterer Airy disk size on the CCD corresponds to ~80μm wide spots on the mirror surface. The crowding observed in high exposure images is due to the size of the Airy disks. The actual scatterers must be sub-micron in size to generate large angle scatter, thus they are actually widely separated within the coating layers of the coating.

It is observed that the shapes of Airy disks at larger exposure times are amplitude-dependent, mostly due to CCD saturation. The effects of saturation are illustrated in Figure 2.

The 40 images analyzed varied in exposure times from 1.25×10^{-4} to 1.3 seconds. The numbers of detected scatterers per image were tabulated and graphed as a function of exposure times in Figure 3. The growth of the number of detected points is compatible with a linear function, with a saturation occurring above 0.2 s exposure. The count saturation was attributed, by manual observation, to crowding of saturated airy disks,

rather than an actual amplitude cutoff of weaker scatterers. It appears that a population of even weaker scatterers, progressively less illuminated in deeper and deeper mirror layers, may lie below the detected ones.

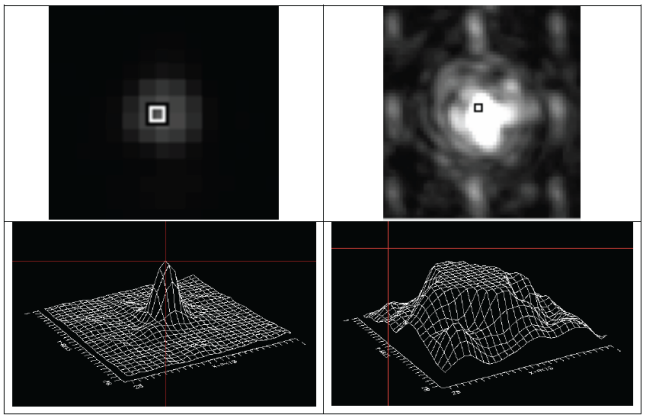

Figure 2. *Images (Top) and Contour Plots (Bottom) of scatterers. A non-saturated Scatterer is shown on the left and an oversaturated one on the right. Saturated scatterers are found with increasing frequency amongst images with longer exposure time.*

III. METHOD LIMITATIONS

Shorter camera exposure times result in a smaller number of scatterers detected, with the less luminous ones fading into the CCD image "dark" pixel count, while the detected scatterers are less saturated with shapes compatible with Airy disks. Longer exposure times proved to be problematic also due to the fact that when the CCD saturation count of 255 is exceeded, there seems to be outflow of the excess charge on the neighboring pixels, as illustrated in Figure 2. To mitigate these shortcomings, it is intended to use a sequence of un-saturated images taken in rapid succession at the same shortened exposure times once more images are available. It is expected that adding the pixel counts of these photos after proper re-centering, to compensate for apparatus movements, and using the camera in "raw data" mode with 14 bit resolution will generate images with much higher-dynamic range, revealing weaker scatterers without saturating the bright ones. A more efficient subtraction of scatterers may be expected from DAOPHOT and a number of fainter scatterers may become visible, thus producing a more reliable luminosity distribution curve. This seemingly obvious solution has a limitation. The signal from very weak scatterers in the TIFF images studied is bundled in the dark count and rounded off to zero, and therefore will never appear in the summed up image.

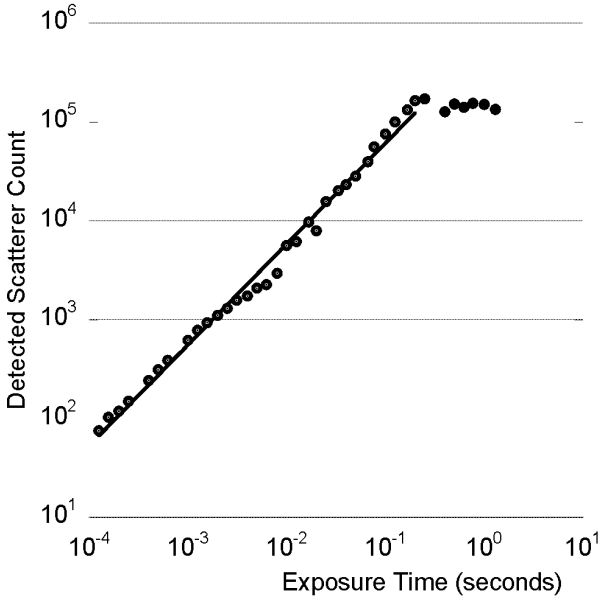

Figure 3. *Detected number of scatterers vs. exposure time: the relationship is nearly linear, with slope ~1, until saturation occurs, as shown by the unitary slope line superimposed on the data (the fit is applied only data below the saturation at 0.2 s).*

The TIFF format used thus far has limited dynamic pixel range of 8-bit depth. "Raw format" images with 14 bit dynamic range, will be utilized in future searches. Studies of images with 14 bit dynamic range show that the dark field forms a narrow peak above zero and therefore will not pile-up on the zero count and rounded off. In this condition even the weakest scatterers will eventually emerge if a sufficient number of images is added up.

At the time this work was written, the two observatories were offline for service upgrades, and the photos with the desired exposure could not be obtained. This work is therefore limited to the best available images.

It should be noted that these scatterers have been observed previously[xii,xiii]. At that time, it was surmised that the scatterers were laser speckle, which is unlikely because the speckle pattern is observed to remain stable even for beam movements over the mirror surface, and speckle patterns do not mimic well the Airy disk patterns that were observed. It is therefore assumed that each Airy disk-like point is the result of point-like scatterers. Interestingly, previous scattered light measurements performed from the same viewports on the initial LIGO mirrors (Fig. 3 of reference XII) found scattered intensity levels in excess of what had been estimated using the known mirror substrate roughness. The scatterers studied here may account for some, or all of that excess power.

It should also be noted that DAOPHOT was already used in angular dependence studies of scattering on sample mirrors[xiii], also finding multiple scatterers throughout the captured images. Angular power information cannot be produced in the measurements described here because the camera was not calibrated in light intensity and all the images were taken from a single location.

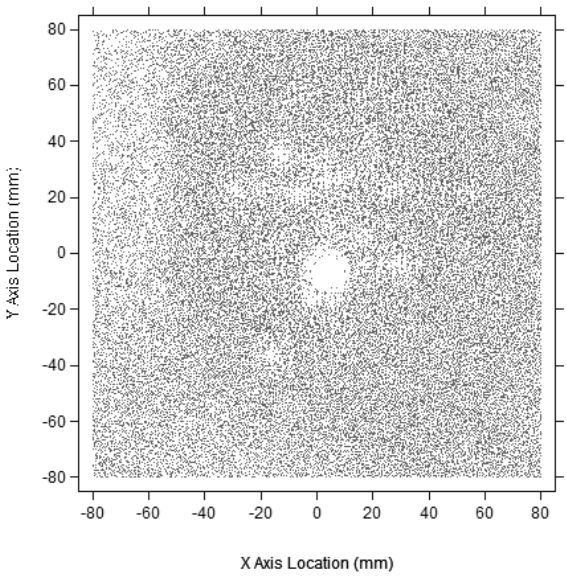

Figure 4: *DAOPHOT-detected scatterers with 0.763 second exposure. Smear due to dirt limits DAOPHOT's detection efficiency in some areas that appear blank. The number of counts per square is reported in table 1. The density of detected scatterers is lower on the beam spot tails, due to the rapidly decreasing illumination, but it is otherwise compatible with a constant value. An average scatterer density of 6.5 scatterer/mm², 10.7 scatterer/mm² at the center, is estimated.*

#	1	2	3	4	5	6	7	8	9	10	Sum
1	1952	1493	1025	1160	1425	1640	1699	1241	1171	1278	**14084**
2	1999	1661	1239	1457	1963	2364	2017	1090	897	1091	**15778**
3	1885	1651	1665	1836	2246	2366	1808	952	736	812	**15957**
4	1695	1485	1945	2267	2691	2471	1734	1087	643	790	**16808**
5	1463	1404	1767	2567	2576	2601	2049	1368	759	812	**17366**
6	1216	1443	1592	2517	2206	2729	2312	1607	850	1048	**17520**
7	934	1462	1431	2487	2539	2626	2249	1891	1231	1480	**18330**
8	977	1444	1270	2502	2645	2286	1629	1731	1593	1888	**17965**
9	1062	1534	1340	2299	2265	1709	1544	1427	1867	2209	**17256**
10	1122	1566	1458	1921	1525	1213	1293	1200	1918	2220	**15436**
Sum	**14305**	**15143**	**14732**	**21013**	**22081**	**22005**	**18334**	**13594**	**11665**	**13628**	**166500**

Table 1: *number of scatterers detected by DAOPHOT in 1.6*

cm × 1.6 cm = 2.56 cm² cells of the image of figure 1. The top line and left column are the column and row number. The bottom line and right column are the row and column sums.

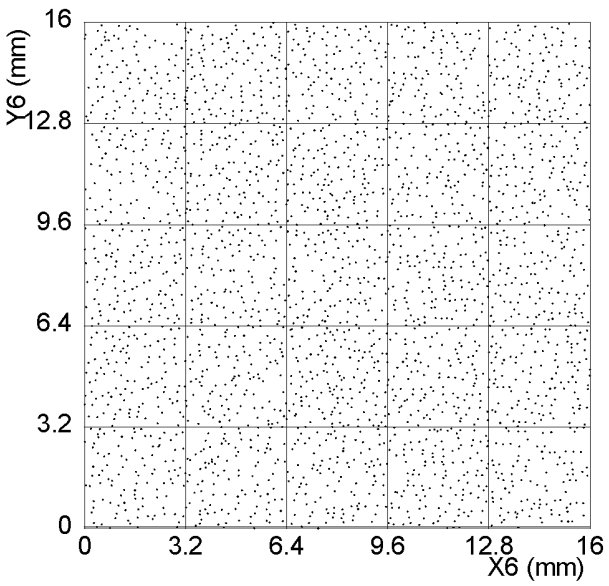

***Figure 5**: scatter plot of the detected scatterers of cell 6,6 of table 1.*

IV. RESULTS

The photographs were taken with approximately 100 kW stored beam illuminating the test masses. The camera utilized a 240mm lens, set at f/11 and ISO 100 with exposure times varying between 1.25×10^{-4} to 1.3 seconds.

Minimum	643
Maximum	2,729
Sum	166,500
Points	100
Mean	1,665
Std Deviation	539
Std Error	54

***Table 2**: Statistical analysis of the data of table 1. The standard deviation of 539 is more than ten times larger than the expected statistical fluctuation, √1665=41, of the mean value, reflecting the masking effects of dirt, and the changing illumination level.*

A pixel size of ~80 μm in both the X and Y directions was calibrated using the known size of straight edges of the mirror support structure, visible in figure 1. Excluding the points where there were smears due to dirt particles degrading the DAOPHOT detection efficiency, the scatterer density around the beam center, at the saturation level of figure 4 (with an exposure time of 0.763 s), was approximately 10.7/mm². The scatter distribution in figure 4 is clearly not uniform, which can be attributed to areas where dirt inhibits DAOPHOT's identification process. This is visible as white patches in figure 4 (bright in figure 1) with a strong deficit of scatterers. The illumination level affects the number of detected scatterers, according to the slope fit in figure 3. The count number is also decreasing on the wings of the stored beam profile, due to lower illumination. It is clear that the average density of scatterer/mm² obtained by dividing the number of points by the field of view area is merely a lower limit.

The following procedure was implemented to produce a better evaluation of the actual scatterers' density if the illumination was uniform and the dirt absent.

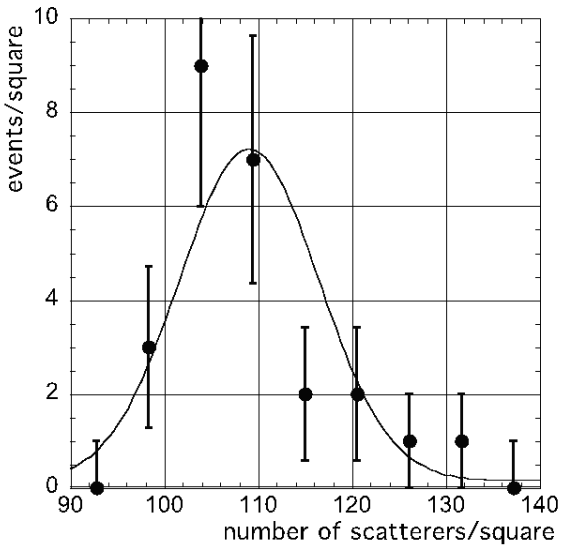

***Figure 6**: Plot of the data of table 3, the data is in agreement, within statistical error bars, with the Gaussian predicted by a uniform distribution of scatterers of average 109 counts/square (smooth line)), 10.7/mm² accounting for the square size.*

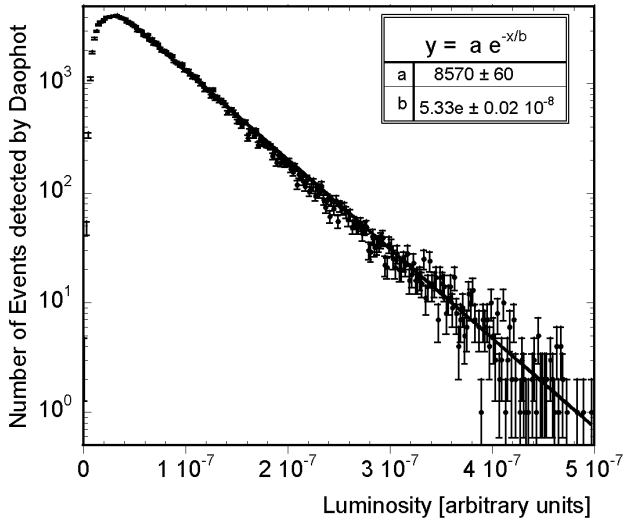

***Figure 7**: Detected scatterer luminosity distribution. The exponential decay fit is performed only on the points above Z=0.5 10⁷.*

Rows / Columns	1	2	3	4	5	Max.	133
1	99	123	99	109	109	Sum	2724
2	99	110	119	103	105	Points	25
3	108	103	105	115	109	Mean	109
4	106	108	133	108	115	Std Dev.	8.5
5	104	104	105	124	102	Std Err.	1.7

***Table 3**: **Left six columns**: number of scatterers detected by DAOPHOT in highest count subdivision of cell 6,6. **Right two columns**: Statistical analysis of the left panel data. The standard deviation of 8.5 counts is in good agreement with the expected statistical fluctuation √109=10.4, indicating that dirt is likely absent in this cell, and the scatterer distribution is uniform.*

The cell region of interest of figure 4 was first sub-divided into a 10 by 10 matrix of smaller cells. The detected scatterers were counted in each of the 100 cells, and reported in Table 1.

Given the fact that dirt masks out detected scatterers and that the beam profile reduces the number of detected scatterers in the wings, the largest value of table 1 is considered to be the best estimator of the undisturbed scatterer density, i.e. the actual detected scatterer density at this exposure level is at least 64% higher than the gross average estimation of 1658 scatterers per bin. It remains to be established if the highest cell count is representative, i.e. unaffected by dirt. It can be considered that, in absence of dirt, the scatterers' distribution should be uniform. If the distribution of scatterers in the bin cell with the highest count is uniform, it is probable that that scatterer is unaffected by dirt.

The highest count is in cell 6,6 in table 1, which is close to the beam center. Cell 6,6 was subdivided into a second 5 x 5 matrix of cells as shown in figure 5, and their content counted. The results are reported in table 3 and figure 6, illustrating the uniform distribution of the scatterers in that cell.

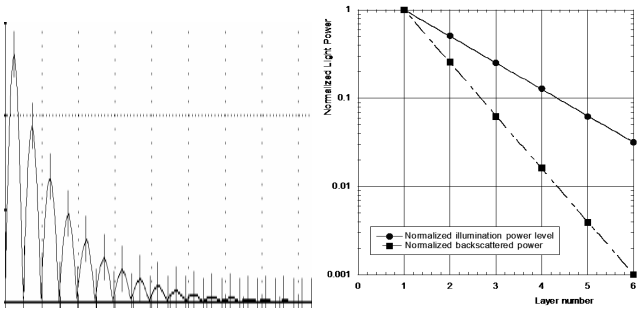

***Figure 8**: **Left:** Calculated electric field intensity within an optimized dichroic advanced LIGO ETM silica/titania-doped-tantala mirror (as in design provided to LMA). **Right:** exponentially decreasing light power as function of layer number (dots). The scattered light is further attenuated on its way back to the surface and the camera. Scatterers beyond the third layer are*

visible at the percent level or less. Therefore, light that is reflected back by the material layers comes from scatterers located in the uppermost coating layers.

The amplitude distribution of the individual events detected by DAOPHOT in the image of 0.763 second exposure is shown in figure 7. It is important to remind that coating layers near the surface are much more strongly illuminated than deeper layers. To make a rough evaluation of the overall number of scatterers actually present throughout the mirror, one should take into consideration the illumination drop with the coating layer number.

In addition, because the camera observation angle from the beam axis is small (9.8°), the backscattered light from deeper layers is reduced by approximately the same factor as the illumination. The two effects amount to a strong exponential attenuation, which makes that scatterers from the second layer are visible with 25% of luminosity and 6.3% from the third layer[xiv]. In practice, assuming that the scatterers are concentrated in the Tantala layers, only scatterers present in the top layers contribute to figure 4 and 5 while scattering from deeper layers is hardly visible. Because there are 26 layers in a coating, about an order of magnitude of additional scatterers can be expected to exist undetected below the surface, i.e. hundreds per square millimeter.

V. Detecting Changes in Optical Scatterer Position and Luminosity and Its Implications

Movements amongst the components of the LIGO apparatus (mirror, beam and camera) are a nuisance for scatterer characterization and need to be corrected before adding up sequences of images. The correction mechanism offers an interesting opportunity. Movements of components can be precisely determined by comparing the image-to-image changing position of scatterers. It is important that non-saturated images be used in this process. The best pair of images available to test this task (images with same exposure were not available in our data set) were two images from the Nov. 2015 data set with 0.125 and 0.1563 milliseconds exposure times, taken approximately 10 seconds apart from one another. Having the choice, 10x or longer exposure would be used. The results obtained here should therefore be considered as upper limits of the achievable resolution.

Using image tracking capabilities in Wolfram Mathematica, the apparent movement of individual detected scatterers were determined.

Figure 9 shows how, when comparing the variations in relative position of detected scatterers of two successive images, one can evaluate the following position sensitivity capabilities.

- The lateral scatter of the points (standard deviation), 10.6 μm in x and 10.8 μm in y, i.e. about 1/10 of a pixel, is the best indicator of the precision of DAOPHOT's positioning for individual, unsaturated scatterers.
- The standard error of the distribution indicates that a beam positioning sensitivity better than 1.28 μm can be achieved. In absence of saturation, this precision can be expected to improve by $1/\sqrt{n}$ where n is the number of detected points. This high precision is important because it allows proper corrections for the image shift when adding the pixel counts from many images.
- The change of the mean value measures the apparent movement of the mirror (the combined relative movement of the camera and mirror). A change of -58±10.6 μm in the x-axis and 31±10.8 μm in the y axis was measured between the two images separated by 10 s intervals.
- Tracking the position of the scatterers does not give information of the beam movements with respect to the mirror surface. In order to accomplish that, one can take advantage of the fact that scatterers are in fixed positions on the mirror surface. Using the luminosity values associated with each detected scatterer, shifts in luminosity within the images were calculated. Dividing the identified scatterers in quadrants, and comparing the four illumination levels integrated over the four quadrants, it is

possible to monitor beam movements across the mirror surface. A split along the x axis was used to detect horizontal motion. Similarly for the vertical one. In the two images studied, the normalized luminosity changed by a factor of 0.0008 along the x axis (from an original ratio -0.0070 to a -0.0062), indicating a leftward shift of the stored beam position. Along the y axis, the luminosity changed by 0.0272 (from an original ratio -0.0278 to -0.0550), indicating a larger upward shift in stored beam position. Supposing a Gaussian beam radius of 50 mm these measurements estimate a "measured" beam to mirror movement of 0.16 and 1.35 mm over a 10 s interval.

The preliminary results above are limited by the fact that the analyzed photos have all different and far-from-ideal exposures. The results from the comparison of the two images used are not sufficient to determine the ultimate position sensitivity, but establish that this kind of analysis can track image-to-image movements and sets an upper limit of the achievable sensitivity even with non optimized exposure times.

These three results represent high-resolution measurements of variables that may be of great interest as feedback signal for improving interferometer controls, or even simply for monitoring.

It is suspected that some of the interferometer glitches that pollute the signal detection pipeline are due to beam movement. It is therefore important, for debugging and reducing false signal probability, to attempt to correlate either of the movements detected with this method with interferometer glitches.

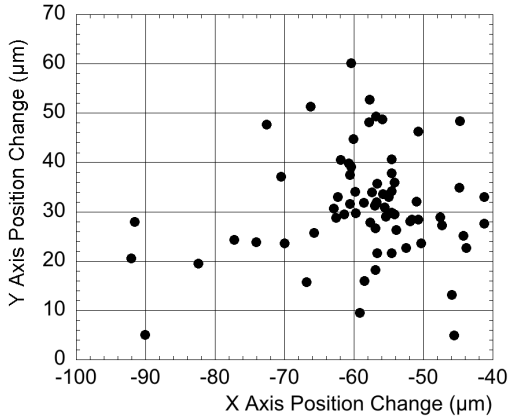

Figure 9*: The above shows the small changes in position detected via Mathematica when comparing two successive ETM images of similar exposure times, taken at a 10 s interval. One pixel is approximately 80 μm in width. Between the two shots, the camera-mirror relative position changed by ~58.48±.10.6 μm in the horizontal position and ~31.07±10.8 μm in the vertical. The image-to-image scatter (fitting error) of the beam center position provided by DAOPHOT is ~1.2-1.3 μm.*

VI. IMPLICATIONS FOR DISSIPATION AND THERMAL NOISES

It is very unlikely that such a high and uniform scatterer density can be accidental. It requires a fundamental source, probably in the deposition process. Vladimir Braginsky[xv,xvi] and Yuri Levin[xvii] predicted that thermal noise of coatings would limit the sensitivity of Gravitational Wave detectors.

Large-angle scatter without absorption require fluctuations of refraction index at sub-wavelength scale. As the chemical composition of the material is uniform, density fluctuations are necessary. Fluctuations of either sign are possible.

Positive refraction index fluctuations are given by crystallites, which are fluctuations with higher molecular order and larger density. Previous studies have shown evidence of large mechanical losses within the coating layer material.[xviii] There, materials are observed to evolve into crystal (columnar) growth in thicker film

depositions of the same materials , as well as in films that have undergone annealing, which imply the presence of crystallite seeds.[xix,xx] The crystallites have a minimum critical size, due to the competition between the high energetic cost of the dangling and frustrated bonds on the surface and the energy gain of crystallization, which is proportional to the volume. Crystallites that are too small tend to dissolve back in the glass during annealing, while larger ones tend to grow. Crystallites can be depressed by alloying different materials, which historically was done to improve coating performance even before this reasoning was developed[iii], or by nano-layering within each coating layer[iv, xx].

Negative refraction index fluctuations are due to local density deficit in the glass. Glasses are always less dense than their crystalline counterpart, due to a statistically uniform distribution of atomic-size voids, but evaporation-deposited glasses are even less dense and can present larger deviations from uniformity. The coating glass appears optically uniform, but one can expect scattering of light from lower density volumes if the void size distribution has sufficiently large fluctuations, and/or if a sufficient concentration of atomic-size voids happens in the scale of a fraction of a wavelength. The ensuing local refraction index deficit could then produce the observed scattering. It is suggested that low density fluctuations may be mitigated by means of hot substrate deposition, ion assisted deposition, annealing or other production techniques.[xxi ,xxii]

While it is impossible to distinguish between high and low density fluctuations with the observational methods used here, both lower and higher density zones are expected to have a larger amount of loose or dangling bonds than the rest of the glass. Both cases can be conceptualized as two-level systems represented by asymmetric double-well potentials in some configuration coordinate. The distribution of corresponding double-wells in the atomic displacement depends on the distribution of bond angles and frustrated bonds in the amorphous material.[xxiii] As an oversimplified picture, one could imagine an atom "flopping" from one side of a bond to the other during stress propagation, thus absorbing energy and dissipating it in the thermal bath. It is clear that these defects can exist on different length and energy scales, ranging from local, atomic-sized defects such as dangling bonds to larger scales such as those that produce two level systems.

The observational method does not allow distinguishing between these two possibilities. Even if one cannot ascertain the exact cause of the fluctuations, they are equally likely sources of the excess of mechanical losses in evaporated glasses. When considering that thermal noise is one of the major sources of noise in gravitational wave detection, the identification of its source has major implications in regards to the optimization of production procedures and ultimately improved reach of the apparatus.[xxiv]

VII. CONCLUSION

The analysis presented here has shown that, when the LIGO test masses are exposed to the high intensity light from the interferometer stored beam, a large and unexpected number of optical scatterers is detected within the mirror coating layers.

Theoretical material science considerations indicate that these scatterers are either nucleation centers, density voids, or a combination of the two, and a likely locus of the anomalous dissipation in the mirror coatings and source of its thermal noise. Observation of these previously overlooked scatterers may point the way towards a mitigation strategy.

The methods developed here allow tracking the motion of the mirrors and the beams on the mirrors, important diagnostic and feedback tools for the observatories.

The background of the detectors could be reduced if some of the glitches were found to correlate with the motions that can be detected with the methods proposed here.

Reduction of thermal noise, reduction of scattering, better alignment, and reduction of glitches are all elements that can potentially increase the detection range of LIGO.

The methods proposed do not give depth information of the scatterers. It is important to precisely and systematically locate the scatterers within the mirror coating thickness, which can perhaps be done with microscope observations.

VIII. ACKNOWLEDGEMENTS

The authors gratefully acknowledge Mara Salvato for suggesting the use of DAOPHOT, without which this work would have been impossible. Hiro Yamamoto is also thanked for his useful comments. Most of the work was performed by undergraduate students as part of the PHYS-470 advanced lab, supervised by LG in the framework of his masters' thesis. The photos analyzed in this work were provided by LIGO. RDS would like to acknowledge that his studies on thermal noise started from discussions and work with Yuri Levin, and later with Vladimir Braginsky. This paper has LIGO Document Number LIGO-P1600325.

IX. FUNDING INFORMATION

National Science Foundation (NSF) (PHY-0757058, PHY-0823459)

[i] Aasi, Junaid, et al. "Advanced LIGO." *Classical and Quantum Gravity* 32.7 (2015): 074001.

[ii] Abbott, B. P., et al. "GW151226: Observation of gravitational waves from a 22-solar-mass binary black hole coalescence." *Physical Review Letters* 116.24 (2016): 241103.

[iii] Harry, Gregory, Timothy P. Bodiya, and Riccardo DeSalvo, eds. *Optical coatings and thermal noise in precision measurement*. Cambridge University Press, 2012.

[iv] Villar, Akira E., et al. "Measurement of thermal noise in multilayer coatings with optimized layer thickness." *Physical Review D* 81.12 (2010): 122001.

[v] M. Principe, "Reflective Coating Optimization for Interferometric Detectors of Gravitational Waves," *Optics Express*. 23.**9** (2015) 10938-10956.

[vi] Harry, Gregory M., and LIGO Scientific Collaboration. "Advanced LIGO: the next generation of gravitational wave detectors." *Classical and Quantum Gravity* 27.8 (2010): 084006.

[vii] Penn, Steven D., et al. "Frequency and surface dependence of the mechanical loss in fused silica." *Physics Letters A* 352.1 (2006): 3-6.

[viii] Levin, Yu. "Internal thermal noise in the LIGO test masses: A direct approach." *Physical Review D* 57.2 (1998): 659.

[ix] Trinastic, Jonathan P., et al. "Molecular dynamics modeling of mechanical loss in amorphous tantala and titania-doped tantala." *Physical Review B* 93.1 (2016): 014105.

[x] Peter B. Stetson, "DAOPHOT: A Computer Program for Crowded-Field Stellar Photometry." *The Astronomical Society of the Pacific*, 99.613 (1987): 191-222

[xi] National Optical Astronomy Observatory (950 N Cherry Ave, Tucson, AZ 85719), https://www.noao.edu/

[xii] William Kells et al., "Scattered Light Loss from LIGO Arm Cavity Mirrors", LIGO Scientific Collaborative Database, LIGO-T0900128 (2009)

[xiii] Joshua Hacker, "Distinguishing Points from Glow in Scattering Images", LIGO Scientific Collaborative Database, LIGO-G1500772 (2015)

[xiv] Orfanidis, Sophocles J. *Electromagnetic waves and antennas*. Rutgers University, 2002.

[xv] Braginsky, V. B., V. P. Mitrofanov, and K. V. Tokmakov. "Energy dissipation in the pendulum mode of the test mass suspension of a gravitational wave antenna." *Physics Letters A* 218.3 (1996): 164-166.

[xvi] V.B. Braginsky, S.P. Vyatchanin, "Corner reflectors and quantum-non-demolition measurements in gravitational wave antennae." *Physics Letters A* V. 324, 5-6 (2004) 345-360.

[xvii] Levin, Yu. "Internal thermal noise in the LIGO test masses: A direct approach." *Physical Review D* 57.2 (1998): 659.

[xviii] Penn, S.D et al. "Mechanical loss in tantala/silica dielectric mirror coatings." *Class. Quantum Grav.* 20.13 (2003)

[xix] Huang-Wei Pan, Shun-Jin Wang, Ling-Chi Kuo, Shiuh Chao, Maria Principe, Innocenzo M. Pinto, and Riccardo DeSalvo, "Thickness-dependent crystallization on thermal anneal for titania/silica nm-layer composites deposited by ion beam sputter method." Optics Express, 22.24 (2014): 29847-29854

[xx] Anders, André. "A structure zone diagram including plasma-based deposition and ion etching." *Thin Solid Films* 518.15 (2010): 4087-4090.

[xxi] Queen, D. R., et al. "Two-level systems in evaporated amorphous silicon." *Journal of Non-Crystalline Solids* 426 (2015): 19-24.

[xxii] Queen, D. R., et al. "Excess specific heat in evaporated amorphous silicon." *Physical review letters* 110.13 (2013): 135901.

[xxiii] M.D. Ediger, "Vapor-deposited glasses provide clearer view of two-level systems," *Proc. Natl. Acad. Sci. U.S.A.* 111.31 (2014): 11232.

[xxiv] Pitkin, M.; Reid, S.; Rowan, S.; Hough, J. Gravitational Wave Detection by Interferometry (Ground and Space). *Living Rev. Relativity (*2011)**,** 14.5.